VIII International Conference on Computational Methods for Coupled Problems in Science and Engineering
COUPLED PROBLEMS 2019
E. Oñate, M. Papadrakakis and B. Schrefler (Eds)

SIMULATION OF MACROSEGREGATION IN LOW-FREQUENCY ELECTROMAGNETIC CASTING BY A MESHLESS METHOD

VANJA HATIĆ [*], BOŠTJAN MAVRIČ [*,†] AND BOŽIDAR ŠARLER [*,†]

[*] Institute of Metals and Technology
Lepi pot 11, 1000 Ljubljana, Slovenia
Web page: https://www.imt.si
[†] Faculty of Mechanical Engineering, University of Ljubljana
Aškerčeva 6, 1000 Ljubljana, Slovenia
Web page: https://www.fs.uni-lj.si/
email: bozidar.sarler@fs.uni-lj.si

Key words: low-frequency electromagnetic casting, macrosegregation, solidification model.

Abstract. The novel use of a meshless numerical approach for simulation of macrosegregation in the low-frequency electromagnetic casting is presented along with the analysis of the simulation results. The casting model includes a coupled set of mass, momentum, energy, and species conservation equations. Lorentz force is computed with the induction equation and used in the solidification model. The coupled physical model is solved in cylindrical coordinate system and can be used to model aluminium alloy billet production. Explicit scheme is used for the temporal discretization, while the meshless diffuse approximate method is used for the spatial discretization. The method is localized with subdomains containing 14 local nodes. The Gaussian weight is used in the weighted least squares minimization. Furthermore, the Gaussian is shifted upstream, when an upwind effect is required in order to increase the convection stability. Direct chill casting under the influence of electromagnetic field (EMF) is simulated for various electric amplitudes and currents. The material properties of Al-5.25wt%Cu are used. The casting parameters and material properties are constant in all presented simulations, while EMF is turned off in some cases in order to study its effect on solidification. The results show that EMF has a large effect on the melt-flow and solidification. Oscillatory, instead of a steady-state, solution is obtained in case of certain geometries in EMF casting. The effect of EMF is hard to predict without the use of numerical simulations, due to strong coupled effects of casting geometry, casting parameters, and EMF parameters. This shows the need for numerical modelling of this strongly coupled problem for its better understanding.

1 INTRODUCTION

Macrosegregation is the chemical inhomogeneity of the composition on the macro-scale level. It is an unavoidable consequence of solidification and one of the major casting defects. It reduces the product quality and is impossible to remove with post-process treatments. The industrial experiments are very expensive and often not possible to perform. That is why the numerical models for prediction of macrosegregation are employed. They can successfully be used to optimize the casting parameters and increase the finished product value. Macrosegregation is caused by various physical phenomena: convection-driven flow,

shrinkage-driven flow, transport of floating grains, deformation-driven flow, and forced flow. The forced flow includes the effect of mechanical, ultrasonic, electromagnetic, etc. stirring and has a very important role in solidification for the low-frequency electromagnetic casting (LFEC).

Complete models for simulation of direct chill casting (DCC), which include mass, momentum, heat, and species transport have been in development for quite a long time. The improvements in the prediction of macrosegregation include: floating grains effect [1], effect of solidification shrinkage [2], multi-component alloys [3], operator splitting scheme [4], and a three-phase model, which includes the effects of intragranular and extragranular liquid [5]. On the other hand, the models for simulation of LFEC have not yet included the prediction of macrosegregation [6]. This is thereby the first investigation of the low-frequency EMF effect on macrosegregation in DCC.

Meshless methods are praised for their flexibility in simplicity of positioning and generation of the computational nodes. Only positions of the computational nodes are required without any other geometrical information. The formulation of the meshless approach is very similar for 2D and 3D, which is a significant benefit in comparison with other numerical methods. Description of the diffuse element method (DEM) is one of the first significant publication on the meshless methods [7]. The diffuse approximation method (DAM), which is employed in the model described in this paper, originates from DEM. The method has successfully been used to solve various thermo-fluid and multi-physics problems [8,9,10].

2 MODEL DESCRIPTION

The volume averaging formulation is used for modelling of the solid-liquid interaction. The conservation equations for mass, energy, momentum, and species are used to model the solidification of aluminium-alloy billets in axisymmetry. The electro-magnetic-induction equation is coupled with the melt-flow. It is used to calculate the magnetic vector potential and the Lorentz force. The Lorentz force is time-averaged and included in the momentum conservation equation, which intensifies the melt-flow. The effect of Joule heating is neglected in the energy conservation due to its insignificant contribution. The semi-continuous casting process is modelled with the Eulerian approach. This implies that the global computational domain is fixed in space. The inflow of the liquid melt is assumed at the top boundary and the outflow of the solid metal is assumed at the bottom. It is assumed that the whole mushy area is a rigid porous media, which is modelled with the Darcy law. Kozeny-Carman relation is used for the permeability definition. The incompressible mass conservation is ensured by the pressure correction, which is performed with the fractional step method. The conservation equations and the induction equation are posed in the cylindrical coordinate system. A linearized eutectic binary-phase diagram is used to predict the solute redistribution in the solid and the liquid phase. The micro model uses the lever rule to determine the temperature and the liquid fraction field from the transport equations.

The solid phase is assumed to be a rigid porous medium, which is traveling with a constant casting speed. The momentum conservation equation is thereby solved only for the liquid phase, which is assumed to be a Newtonian fluid:

$$\frac{\partial}{\partial t}\left(\rho g_l \left\langle \mathbf{v}_l \right\rangle^l\right)+\nabla\cdot\left(\rho g_l \left\langle \mathbf{v}_l \right\rangle^l \left\langle \mathbf{v}_l \right\rangle^l\right)=-g_l\nabla\left\langle p_l \right\rangle^l-{g_l}^2\frac{\mu_l}{K}\cdot\left(\left\langle \mathbf{v}_l \right\rangle^l-\mathbf{v}_{cast}\right)+g_l\mu_l\nabla\cdot\left[\nabla\left(g_l\left\langle \mathbf{v}_l \right\rangle^l\right)+\left(\nabla\left(g_l\left\langle \mathbf{v}_l \right\rangle^l\right)\right)^T\right]+g_l\mathbf{b}^{EM}+\rho g_l\mathbf{g}\left[1+\beta^T\left(T^{ref}-T\right)+\beta^C\left(C^{ref}-\left\langle C_l \right\rangle^l\right)\right], \tag{1}$$

where t, ρ, μ_l, β^T, β^C, K, $\mathbf{g}$, g_l, $\left\langle \mathbf{v}_l \right\rangle^l$, $\mathbf{v}_{cast}$, $\left\langle p_l \right\rangle^l$, T^{ref}, T, C^{ref}, and $\mathbf{b}^{EM}$ are time, density, liquid viscosity, thermal expansion coefficient, species expansion coefficient, permeability, gravity acceleration vector, volume fraction of liquid, intrinsic liquid velocity, casting velocity, intrinsic liquid pressure, reference temperature, temperature, reference concentration, liquid intrinsic concentration, and time-averaged Lorentz force, respectively. The simple Chorin's pressure-correction scheme is used to ensure the mass conservation.

Local thermal equilibrium is assumed in the heat transport equation:

$$\frac{\partial}{\partial t}\left(h_m\right)+\nabla\cdot\left(g_s\left\langle h_s \right\rangle^s\mathbf{v}_{cast}\right)+\nabla\cdot\left(g_l\left\langle h_l \right\rangle^l\left\langle \mathbf{v}_l \right\rangle^l\right)=\nabla\cdot\left(\frac{\lambda_m}{\rho}\nabla T\right) \tag{2}$$

where λ_m, h_m, $\left\langle h_s \right\rangle^s$, and $\left\langle h_l \right\rangle^l$ are thermal conductivity, volume-averaged enthalpy, intrinsic enthalpy of the solid phase, and intrinsic enthalpy of the liquid phase, respectively.

Diffusivity is neglected in both phases in the species transport equation:

$$\frac{\partial}{\partial t}\left(C_m\right)+\nabla\cdot\left(g_s\left\langle C_s \right\rangle^s\mathbf{v}_{cast}\right)+\nabla\cdot\left(g_l\left\langle C_l \right\rangle^l\left\langle \mathbf{v}_l \right\rangle^l\right)=0 \tag{3}$$

where C_m, $\left\langle C_s \right\rangle^s$, and $\left\langle C_l \right\rangle^l$ are volume-averaged concentration, intrinsic concentration of the solid phase, and intrinsic concentration of the liquid phase, respectively.

The electromagnetic field is calculated with the induction equation:

$$\nabla^2\mathbf{A}=\mu_0\sigma\frac{\partial\mathbf{A}}{\partial t}-\mu_0\sigma\mathbf{v}\times\left(\nabla\times\mathbf{A}\right)-\mu_0\mathbf{J}_{ext} \tag{4}$$

where $\mathbf{A}$, $\mathbf{J}_{ext}$, $\mathbf{v}$, μ_0, and σ are magnetic vector potential, external electric current density, volume-averaged velocity, magnetic permeability of free space, and electrical conductivity, respectively. The current density is the source term, which is calculated from the coil specifications. Harmonic time dependence of magnetic vector potential and current density is imposed. Time-averaged Lorentz force is then calculated as the cross product of the steady parts of current density $\mathbf{J}_0$ and magnetic field $\mathbf{B}_0$:

$$\mathbf{b}^{EM}=-\frac{1}{2}\mathrm{Re}\left(\mathbf{J}_0\times\mathbf{B}_0\right) \tag{5}$$

3 NUMERICAL METHOD

The partial differential equations are solved with the meshless-diffuse-approximate method. The DAM uses the weighted least squares to determine a locally smooth approximation ($\hat{f}$)

from a discrete set of data:

$$\hat{f}(\mathbf{x}) = \mathbf{p}(\mathbf{x}, \mathbf{x}_0)\boldsymbol{\alpha} = \sum_{j=1}^{J} p_j(\mathbf{x}, \mathbf{x}_0)\alpha_j \tag{6}$$

where $\boldsymbol{\alpha}$ is the vector of coefficients and $\mathbf{p}(\mathbf{x}, \mathbf{x}_0)$ is the vector of J trial functions. The second-order polynomials are used as trial functions. The Gaussian is used as the weight function in the minimization expression:

$$\theta(\mathbf{x}, \mathbf{x}_0) = \exp\left(-c\frac{\|\mathbf{x}-\mathbf{x}_0\|^2}{h^2}\right), \tag{7}$$

where c and h are free-parameter and scaling factor, which are equal to 5 and to the Euclidian distance between $\mathbf{x}_0$ and the farthest positon from $\mathbf{x}_0$ in the discrete set of data.

The method is localized by defining the smooth approximation for each computational node separately. This is performed by associating each node with an unique local neighbourhood, which is used for minimization. 14 nodes are included in the local subdomains for DCC and LFEC simulations. The stability of the advective term is attained with a shift of the Gaussian weight and evaluation location in the upwind direction. This approach is called adaptive upwind weight function and it is confirmed that is a very successful stabilization procedure [11]. Explicit Euler scheme is used for temporal discretization.

4 SIMULATIONS

Simulations are performed for low-frequency electromagnetic casting process of Al-5.25wt%Cu alloy. Material properties are calculated with the JMatPro software. The secondary dendrite arm spacing is estimated from the literature [12]. The casting temperature and velocity are set to 680 °C and 120 mm/min, respectively. The initial cooling water temperature and discharge are set to 25 °C and 6 m^3/h, respectively. The coil is wrapped around the billet and positioned 0.05 m from the billet surface at z = 0 m. The coil has 40 turns, while the total cross-section area of the windings is $9 \cdot 10^{-4}$ m^2. The electric current magnitude and frequency are varied in the computational cases and are presented in Table 1.

Table 1: EMF parameters of the simulated cases.

Case	I [A]	f [Hz]
LFEC0	100	10
LFEC1	50	10
LFEC2	150	10
LFEC3	100	5
LFEC4	100	20

The casting geometry resembles the realistic industrial geometry and is described by the boundary parametrization points, which are displayed in Figure 1. The length of the billet is limited to 0.9 m, which is enough to reach the steady-state conditions at the outflow.

Symmetry boundary conditions are used at the west boundary. Velocity is set to zero at the

east boundary, while the adiabatic conditions are assumed for the species transport. Robin type of boundary condition is used for heat transfer in all three regions of the east boundary. Heat transfer coefficient is determined differently for each of the three regions; the hot-top is thermally insulated, HTC in the mould-chill depends on the liquid fraction, and HTC in the direct-chill is calculated with the Weckman-Niessen relation [13]. Dirichlet boundary conditions are assumed at the top boundary, where the initial species value and casting temperature are prescribed. A developed Poisseuille flow is assumed for the liquid velocity. Velocity at the bottom boundary is constant and equal to the casting speed. The heat and species conduction at the bottom boundary are both set to zero.

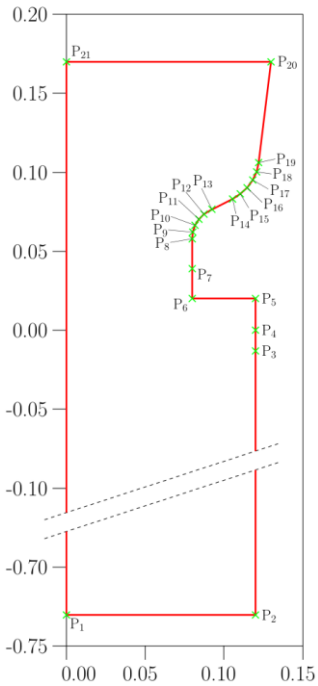

Figure 1: Parametrisation of the domain boundary.

Variable-density adaptive computational node arrangement is used in simulations. The finest node spacing is used in the mushy zone (r_0=0.32 mm), while the coarsest is in the solid (r_0=10.0 mm). Approximately 85,000 computational nodes are used for computation of mass, momentum, heat, and species transfer. An extended computational domain, which includes approximately 210,000 nodes, is used for computation of the induction equation.

5 RESULTS

In contrary to DCC simulations, the results of LFEC simulations do not always reach a steady-state. An oscillating pattern is observed, where the time interval depends on EMF parameters and the casting geometry. A repeating pattern can roughly be determined by observation of the melt flow structure throughout the simulation. Duration of a single interval is equal to 18.5 s, 9.1 s, and 28.0 s for LFEC0, LFEC2, and LFEC3, respectively. A steady state is achieved for LFEC1 and LFEC4. During a single interval the vortices are broken down in

several smaller ones and reconnected into larger ones (see Figure 2). Although the size, position, and structure of the vortices are not exactly repeated in each interval, it is similar enough to cause a repeating pattern in other fields.

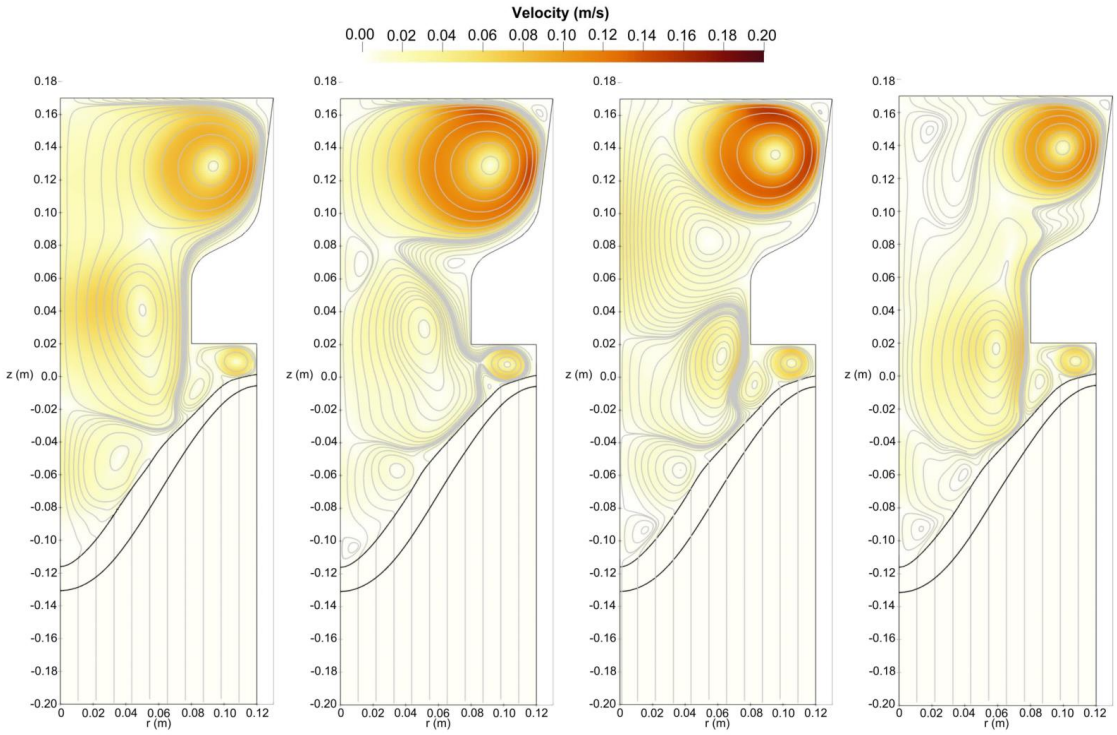

(A) $t_{\mathrm{int}} = 0\,\mathrm{s}$ (B) $t_{\mathrm{int}} = 6\,\mathrm{s}$ (C) $t_{\mathrm{int}} = 10\,\mathrm{s}$ (D) $t_{\mathrm{int}} = 17\,\mathrm{s}$

Figure 2: Transient results for the mixture velocity for geometry LFEC0.

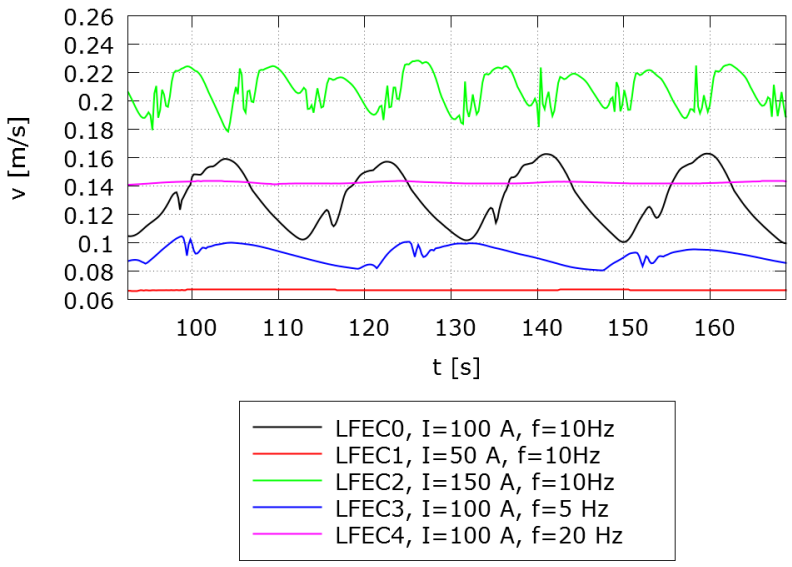

Figure 2: Time evolution of the maximum velocity in the billet for all cases.

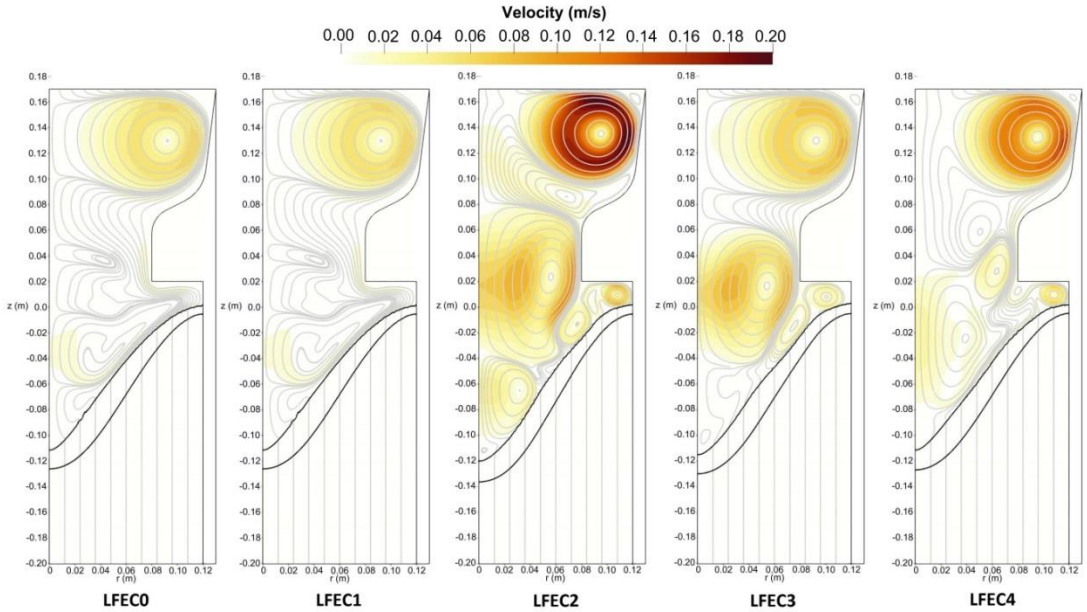

Figure 3: Comparison of the mixture velocity for a single snapshot for all simulation cases.

A decrease and increase of the current amplitude result in a decrease and increase of the maximum velocity, respectively (see Figure 2 and 3). The melt flow in LFEC1 has a reduced amount of vortices. The smaller intensity of the flow results in a steady state without the oscillatory instabilities. The maximum velocity in LFEC2 is almost doubled, while the flow intensity and the frequency of the instabilities are increased. Both simulations with the modified electric frequency result in less pronounced oscillations. The amplitude of the maximum velocity is greatly reduced in the LFEC3 case.

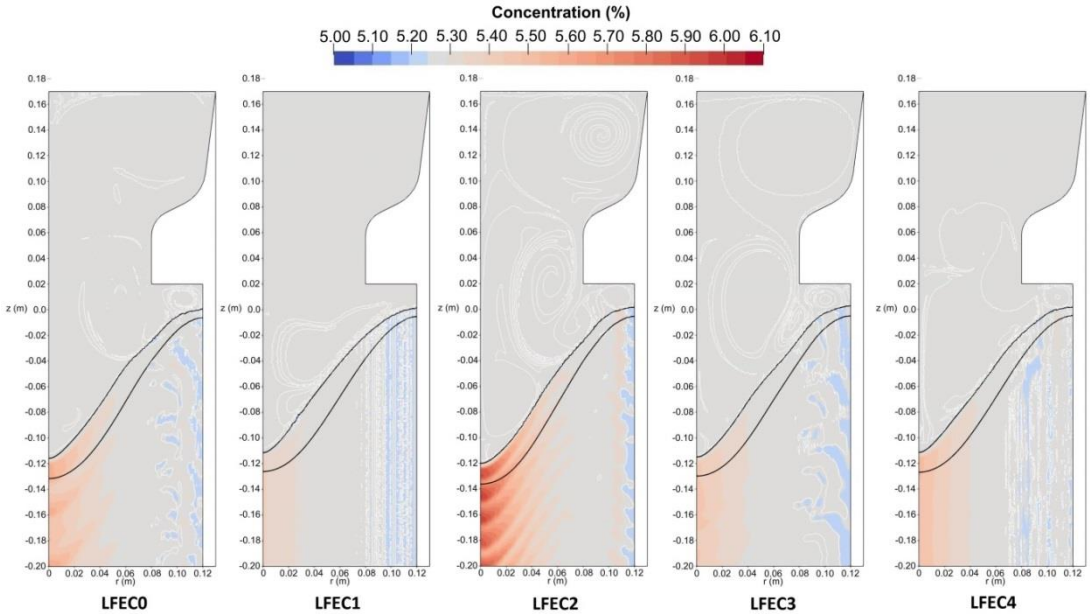

Figure 4: Comparison of the concentration field for a single snapshot for all simulation cases.

Especially the effect on the concentration field is of great interest. From the contour plot (see Figure 4) it is observed that concentration in the solid along the z-axis is not constant when unsteady conditions are met, which is contrary to what is observed in DCC. Instead, a repeating pattern is formed along the vertical direction.

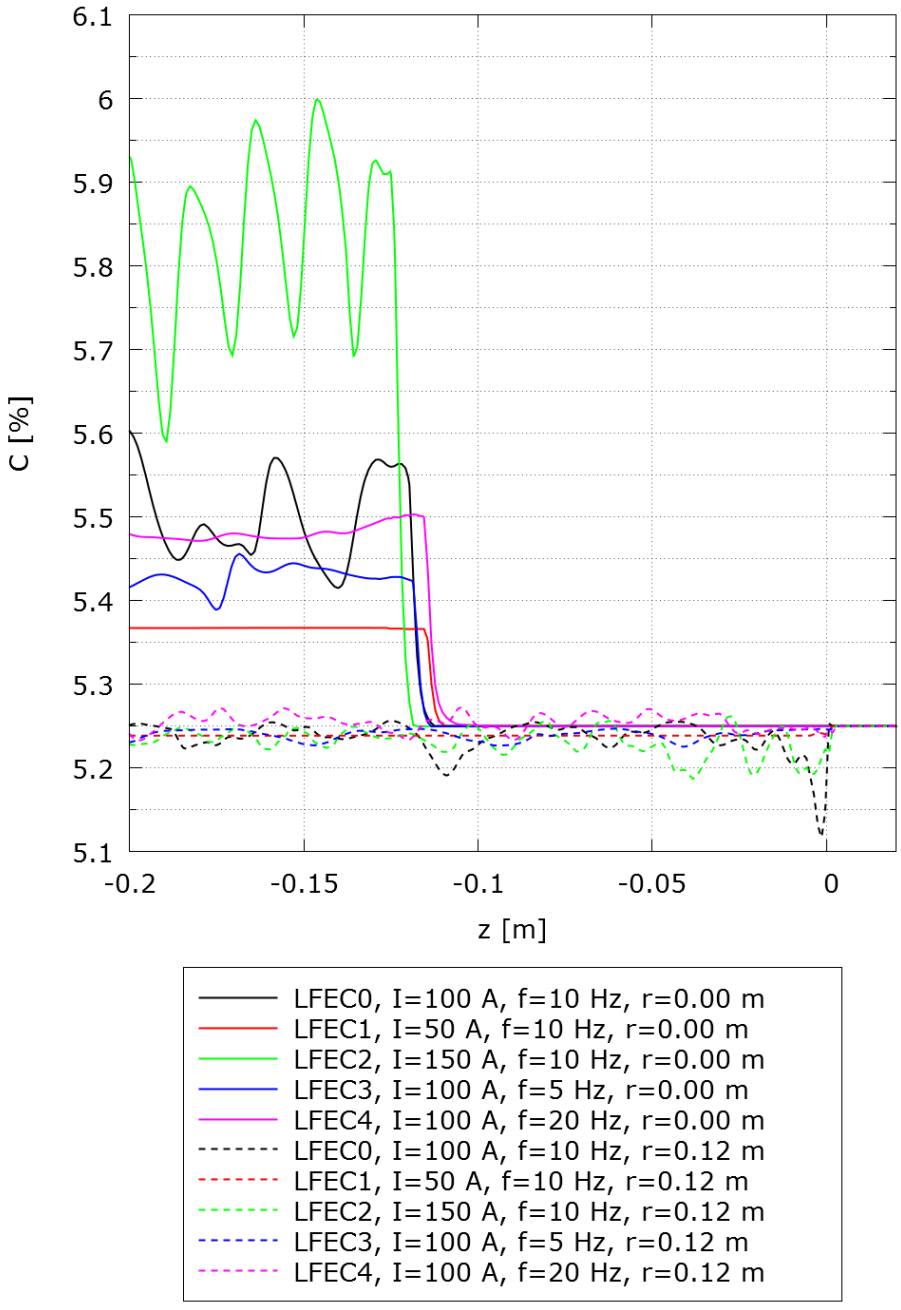

Figure 5: Concentration field for vertical cross sections at the billet center and surface.

Due to fluctuations in the solid species it is hard to quantify macrosegregation, which is usually displayed with horizontal cross section in the solid. But this would not be representative for comparison in the case of unsteady conditions. The comparison of the results for different geometries is therefore made for the vertical cross-sections at the center (r=0 m) and at the surface (r=0.12 m) of the billet (see Figure 5). Macrosegregation in the center fluctuates with different frequency and amplitude for each simulated case. Amplitude is largest in LFEC2 and smallest in LFEC1. This corresponds to the maximum velocities observed in the liquid melt. Furthermore, since a steady-state is achieved in LFEC1 and LFEC4, macrosegregation profile along the z-axis is constant in the solidified part of the billet.

6 FINDINGS

Computer simulations of low-frequency electromagnetic casting of Al-5.25wt%Cu alloy are performed with the mathematical model presented in the 2nd and 3rd section of this paper. The effect of EMF parameters in LFEC on melt flow and macrosegregation is evaluated. It is observed that the electric current frequency and intensity have a substantial effect on solidification in LFEC. There is a small effect on temperature distribution and the sump shape, but the effect on the melt flow and macrosegregation is extensive.

By comparing the simulations it can be concluded that an increase in amplitude and frequency of the maximum velocity results in an increase of amplitude and frequency of the macrosegregation evolution. The results show that it is not possible to make any general conclusions about the direct impact of the EMF parameters on macrosegregation formation. The problem is of such complexity that it is seems impossible to predict the melt flow structure and the macrosegregation without numerical simulations or industrial trials.

REFERENCES

[1] Ni, J. and Beckermann, C. A volume-averaged two-phase model for transport phenomena during solidification. *Metallurgical Transactions B* (1991) **22(3)**: 349-361.

[2] Reddy, A.V. and Beckermann, C. Modeling of macrosegregation due to thermosolutal convection and contraction-driven flow in direct chill continuous casting of an Al-Cu round ingot. *Metallurgical and Materials Transactions B* (1997) **28(3)**: 479-489.

[3] Krane, M.J.M., Incropera, F.P., and Gaskell, D.R. Solidification of ternary metal alloys - I. Model development. *International Journal of Heat and Mass Transfer* (1997) **40(16)**: 3827-3835.

[4] Založnik, M. and Combeau, H.. An operator splitting scheme for coupling macroscopic transport and grain growth in a two-phase multiscale solidification model: Part I - Model and solution scheme. *Computational Materials Science* (2010) **48(1)**: 1-10.

[5] Heyvaert, L., Bedel, M., Založnik, M., and Combeau, H. Modeling of the Coupling of Microstructure and Macrosegregation in a Direct Chill Cast Al-Cu Billet. *Metallurgical and Materials Transactions A* (2017) **48(10):** 4713-4734.

[6] Hatić, V., Mavrič, B., Košnik, N., and Šarler, B. Simulation Of Direct Chill Casting Under The Influence Of A Low-Frequency Electromagnetic Field. *Applied Mathematical Modelling* (2018) **54**: 170-188.

[7] Nayroles, B., Touzot, G., and Villon, P. Generalizing the finite element method: Diffuse approximation and diffuse elements. *Computational Mechanics* (1992) **10(5)**: 307-318.

[8] Sadat, H. and Prax, C. Application of the diffuse approximation for solving fluid flow and heat transfer problems. *International Journal of Heat and Mass Transfer* (1996) **39(1)**: 214-218.
[9] Šarler, B., Vertnik, R., and Perko, J. Application of diffuse approximate method in convective-diffusive solidification problems. *Computers, Materials & Continua* (2005) **2(1)**: 77-83.
[10] Talat, N., Mavrič, B., Hatić, V., Bajt, S., and Šarler, B. Phase field simulation of Rayleigh–Taylor instability with a meshless method. *Engineering Analysis with Boundary Elements* (2018) **87:** 78-89.
[11] Hatić, V., Mavrič, B., and Šarler, B. Simulation of a macrosegregation benchmark with a meshless diffuse approximate method. *International Journal of Numerical Methods for Heat & Fluid Flow* (2018) **28(2)**: 361-380.
[12] Eskin, D.G., Savran, V.I., and Katgerman, L. Effects of melt temperature and casting speed on the structure and defect formation during direct-chill casting of an Al-Cu alloy. *Metallurgical and Materials Transactions A* (2005) **36**: 1965-1976.
[13] Weckman, D.C. and Niessen, P. A numerical simulation of the D.C. continuous casting process including nucleate boiling heat transfer. *Metallurgical Transactions B* (1982) **13(4)**: 593-602.